Stable analytical inversion solution for processing lidar returns

James D. Klett

A simple analytical method is presented that shows some potential for application to the problem of extracting attenuation and backscatter coefficients in an inhomogeneous atmosphere from the return signal of a monostatic single-wavelength lidar system. The method assumes the validity of the single-scattering lidar equation and a power law relationship between backscatter and attenuation. For optical depths greater than unity the inversion method can be applied in principle using only information contained in the signal itself. In contrast to a well-known related analytical inversion solution, the new solution form is shown to be stable with respect to perturbations in the signal, the postulated relationship between backscatter and attenuation, and the assumed or estimated boundary value of attenuation.

I. Introduction

An early and continuing goal of lidar research has been to devise an inversion method whereby profiles of optical parameters such as attenuation and backscatter coefficients in an inhomogeneous atmosphere can be quickly and accurately deduced from the return signal of a monostatic single-wavelength lidar system. This is a problem area where, as expressed by Collis and Russell in an excellent review article, "... the early promise of lidar has not yet been fulfilled." [1] Some of the difficulties encountered along the way have been due to limitations in lidar performance and associated data processing technology, while others follow from theoretical requirements and constraints peculiar to the inversion process. This article addresses some aspects of the latter category of problems and presents in particular a simple inversion method based on a new form of a well-known analytical solution.

II. Review of the Slope and Solution Methods of Inversion

For a monostatic single-wavelength pulsed lidar, the assumed basic governing form is the single-scattering lidar equation:

$$P(r) = P_0 \frac{c\tau}{2} A \frac{\beta(r)}{r^2} \exp\left[-2\int_0^r \sigma(r')dr'\right], \tag{1}$$

where $P(r)$ is the instantaneous received power at time t, P_0 the transmitted power at time t_0, c the velocity of light, τ the pulse duration, A the effective system receiver area, $r[= c(t - t_0)/2]$ is the range, and $\beta(r)$ and $\sigma(r)$ are, respectively, the volume backscatter and attenuation coefficients of the atmosphere. A more convenient signal variable is the logarithmic range-adjusted power, defined as

$$S(r) \equiv \ln[r^2 P(r)]. \tag{2}$$

In terms of $S = S(r)$ and $S_0 = S(r_0)$, where r_0 is a given constant reference range, Eq. (1) may be expressed in a system-independent form:

$$S - S_0 = \ln\frac{\beta}{\beta_0} - 2\int_{r_0}^r \sigma dr', \tag{3}$$

where $\beta_0 = \beta(r_0)$.

The differential equation corresponding to Eq. (3) is

$$\frac{dS}{dr} = \frac{1}{\beta}\frac{d\beta}{dr} - 2\sigma, \tag{4}$$

a solution to which evidently requires knowing or assuming a relationship between β and σ whenever $d\beta/dr \neq 0$. On the other hand, if the atmosphere is homogeneous so that $d\beta/dr = 0$, the attenuation coefficient can be expressed directly in terms of the signal slope:

$$\sigma_{\text{hom}} = -\frac{1}{2}\frac{dS}{dr}. \tag{5}$$

This is the basis of the slope method of inversion,[2,3] in which typically the slope of the least squares straight line fit to the curve $S = S(r)$ is used as the best estimate of dS/dr over any interval where S itself appears to be nearly a straight line.

Going a step further, it has often been assumed that since the atmosphere is more likely to be homogeneous

When this work was done the author was with New Mexico State University, Physical Science Laboratory, Box 3-PSL, Las Cruces, New Mexico 88003. He is now at Areté Associates, P.O. Box 350, Encino, California 91316.

Received 14 April 1980.
0003-6935/81/020211-10$00.50/0.

over small rather than large intervals, by applying the slope method to a succession of small intervals a reasonable first approximation to $\sigma = \sigma(r)$ in a notably inhomogeneous atmosphere may also be achieved. From Eq. (4) it is clear that this amounts to a conjecture that generally $\beta^{-1}|d\beta/dr| \ll 2\sigma$, at least over most of the S curve. Unfortunately, assumptions like this appear not to be well justified for many situations of interest, e.g., under conditions of dense cloud, fog, smoke, and dust. Even under the relatively stable conditions prevailing in fogs, significant local heterogeneities occur. For example, the spatial variation of fog drop concentrations is often quite large, ranging up to 2 orders of magnitude for certain size categories.[4,5] Such microstructure variation along the lidar beam path could easily lead to relatively large fluctuations in $d\beta/dr$, hence invalidating local application of the slope method. The same criticism applies to the so-called ratio or slice method of inversion,[6,7] which is merely an extremely close variant of the slope method as applied to successive range intervals. (Additional discussion on the merits of the slope and ratio methods is available through the recent articles of Kohl[8,9] and Brown.[10])

Several observational and theoretical studies have been published that show that under a wide range of circumstances for which particulate backscattering dominates that due to atmospheric gases (i.e., roughly for hazy, cloudy, or foggy conditions and generally for IR wavelengths), β and σ can in fact be related approximately according to a power law of the form

$$\beta = \text{const}\ \sigma^k, \tag{6}$$

where k depends on the lidar wavelength and various properties of the obscuring aerosol. Reported values of the exponent are generally on the interval $0.67 \leq k \leq 1.0$.[11–15] If such a relationship is assumed, Eq. (4) becomes

$$\frac{dS}{dr} = \frac{k}{\sigma}\frac{d\sigma}{dr} - 2\sigma. \tag{7}$$

Although the above ordinary differential equation is nonlinear, it nevertheless has an elementary structure, namely that of the Bernoulli or homogeneous Ricatti equation.[16] For a very long time (nearly 300 years) it has been known that equations of this type may be transformed to a first-order linear form by introducing a new unknown equal to the reciprocal of the original. The general solution can therefore be easily written as

$$\sigma^{-1} = \exp\left(-\int^r \frac{1}{k}\frac{dS}{dr'}\,dr'\right) \times \left[C - 2\int^r \frac{\exp}{k}\left(-\int^{r'}\frac{1}{k}\frac{dS}{dr''}\,dr''\right)dr'\right], \tag{8}$$

where C is the integration constant. If k is regarded as constant, which appears not to be unduly restrictive and shall be assumed here for brevity, a well-known form of the solution may be obtained:

$$\sigma = \frac{\exp[(S - S_0)/k]}{\left\{\sigma_0^{-1} - \frac{2}{k}\int_{r_0}^r \exp[(S - S_0)/k]dr'\right\}}, \tag{9}$$

where $\sigma_0 = \sigma(r_0)$. The first appearance of Eq. (9) or its equivalent in the literature on remote sensing was apparently in 1954 in the context of rain intensity measurements by radar at attenuating wavelengths.[17] It has since reemerged in several articles on the interpretation of lidar measurements.[3,18–20]

In spite of the evident theoretical superiority of Eq. (9) over the slope method [which corresponds to setting $k = 0$ in Eq. (7)], it is the latter method that is most often used. This is because Eq. (9) has a tendency to produce at best marginal results, and in practice has likely been more a source of frustration than a useful tool for analyzing radar or lidar returns. For example, in their 1954 article referred to above, Hitschfeld and Bordan[17] concluded it was probably not possible to calibrate a radar set accurately enough to make use of the solution, and that rainfall measurements made without correcting for attenuation via the solution are in many cases more accurate than the corrected values. Worse yet, others have noted the solution may lead to "... absurdly large, infinite, or negative values ..." [18] and "... physically meaningless ..." [21] results. Others have avoided such behavior only by using unrealistically large values of k.[3]

There is surprisingly little comment in the literature on the reasons for the failure of Eq. (9). It seems only to be somewhat vaguely attributed to the omission of multiple-scattering effects.[1,7] However, since the slope method suffers from the same deficiency, but with apparently much less drastic consequences, this explanation is not very convincing.

Unfortunately, only a few relevant studies on the possible importance of multiple scattering are available. In one of these, Viezee *et al.*[7] compared lidar and transmissometer measurements in dense fog and found an apparent 10–45% overprediction of lidar-derived visibilities using the slope method. They conjectured this discrepancy was due to the influence of forward and multiple scattering and proposed an empirical correction to the slope method for use under turbid atmosphere conditions. On the other hand, they also noted that available theoretical descriptions of multiple scattering[22–24] could not account for the observed discrepancies in the lidar and transmissometer data. A later Monte Carlo simulation of second- and third-order multiple scattering in dense homogeneous fog led to the conclusion that multiply scattered radiation will cause the slope method to be in error by less than ~10% for visibilities of the order of 100 m.[25]

From these studies it appears unlikely that even for a dense dispersion the contribution of multiply scattered radiation could make a crucial difference in the applicability of Eqs. (1) or (9). Therefore, although it would certainly be desirable to replace Eq. (1) with a new governing form containing higher scattering approximations (perhaps, for example, along the lines recently outlined by Samokhvalov[26]), there seems at present no justification for regarding the inclusion of multiply scattered radiation effects as the *sine qua non* for the inversion of lidar signals from a markedly inhomogeneous atmosphere.

From a purely mathematical point of view, it is easy to see the problem with Eq. (9). Since on average the signal decays with range beyond r_0 due to attenuation, σ is determined as the ratio of two numbers, which each become progressively smaller with increasing r; furthermore, the denominator, which must approach zero at nearly the same rate as the numerator, is expressed as the difference between two relatively large numbers. Such structure produces a strong tendency for instability and suggests that unattainable accuracy in the determination of σ_0 may often be requisite for avoiding a singularity, even for signals that are free of noise.

The above description may be illustrated quantitatively by considering the growth of a small perturbation in σ due to an error δ_0 in the determination of σ_0. For the same signal let σ be the solution corresponding to σ_0 and $\sigma' = \sigma + \delta$ be the solution corresponding to $\sigma_0' = \sigma_0 + \delta_0$. Then from the integrated form of Eq. (7) it follows that

$$S - S_0 = k \ln \frac{\sigma}{\sigma_0} - 2 \int_{r_0}^{r} \sigma dr = k \ln \frac{\sigma'}{\sigma_0'} - 2 \int_{r_0}^{r} \sigma' dr, \qquad (10)$$

which implies

$$(1 + \delta/\sigma) = (1 + \delta_0/\sigma_0) \exp\left(\frac{2}{k} \int_{r_0}^{r} \delta dr\right). \qquad (11)$$

For simplicity consider a homogeneous atmosphere with $\sigma = \sigma_0$. Then by differentiating Eq. (11) one obtains

$$\frac{d\zeta}{dr} = \frac{2}{k} \sigma_0 \zeta(\zeta - 1),$$

where $\zeta = (1 + \delta/\sigma_0)$. This is a homogeneous Ricatti equation, like Eq. (7), with a solution given by

$$\left(1 + \frac{\delta}{\sigma_0}\right)^{-1} = 1 - \frac{\delta_0}{\sigma_0}\left(1 + \frac{\delta_0}{\sigma_0}\right)^{-1} \exp\left[\frac{2\sigma_0(r - r_0)}{k}\right]. \qquad (12)$$

From this expression it can be seen that an underestimate of σ ($\delta_0 < 0$) leads to $\delta \to -\sigma_0$ (i.e., $\sigma \to 0$) as $r \to \infty$. On the other hand, if σ_0 is overestimated ($\delta_0 > 0$), $\sigma \to \infty$ within a finite distance given by

$$\Delta r = \frac{k}{2\sigma_0} \ln\left(1 + \frac{\sigma_0}{\delta_0}\right). \qquad (13)$$

For example, if $\sigma_0 = 10\ \text{km}^{-1}$, $k = 1$, and $\delta_0/\sigma_0 = 10^{-2}$, the solution has a singularity within about the next 231 m; also, for $r > r_0 + \Delta r$ the solution is negative. This example is also shown in Fig. 1, where the unit of length for range plotted along the abscissa has been set equal to 0.003 km (3 m), and attenuation per kilometer is plotted along the ordinate. [This same choice of units is used for all the theoretical curves of $\sigma = \sigma(r)$ given in this paper. Corresponding curves of $S - S_0$ vs $r - r_0$ use the same range scale; $S - S_0$ is of course dimensionless.] The tendencies shown in Fig. 1 are accentuated by larger σ_0/k (lower visibilities) and larger δ_0/σ_0 (poorer estimates of σ_0).

Finally, substitution of Eq. (12) back into Eq. (10) reproduces the original signal, $S - S_0 = -2\sigma_0(r - r_0)$, independently of the value of δ_0. Therefore, two main points should be emphasized regarding these results: (1) Equation (9) is—to paraphrase loosely a terminology used in analogous, although generally more complicated circumstances—ill constructed, in that small differences

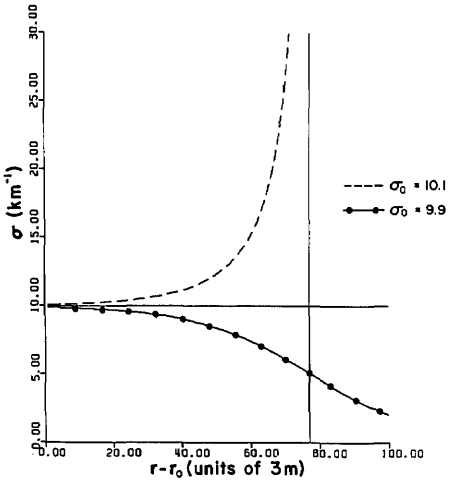

Fig. 1. Growth of perturbations in σ due to small errors in the determination of σ_0.

in the choice of boundary value σ_0 provide no assurance that the corresponding solutions will remain close for $r > r_0$. (2) Closeness of the $S(\sigma)$ curve, reconstructed from the solution for σ, to the original S curve is insufficient to guarantee the reasonableness of the solution. (Such closeness has been used in the past as a test of validity of the solution.[3]) Because of this behavior one would expect, and experience has shown, that Eq. (9) by itself is of very little practical value.

III. New Solution Form

It is fortunately quite easy to select a different and more appropriate solution form than Eq. (9). One merely has to evaluate the integration constant C in Eq. (8) in terms of a reference range r_m so that the solution is generated for $r \le r_m$ rather than for $r \ge r_0$ as before. For constant k the result is

$$\sigma(r) = \frac{\exp[(S - S_m)/k]}{\left\{\sigma_m^{-1} + \frac{2}{k} \int_{r}^{r_m} \exp[(S - S_m)/k] dr'\right\}}, \qquad (14)$$

where $S_m = S(r_m)$ and $\sigma_m = \sigma(r_m)$. This seemingly innocuous change from Eq. (9) makes a very significant difference in the behavior of the solution. As r decreases from r_m, σ is now determined as the ratio of two numbers that each become progressively larger, so that stability and accuracy are easy to maintain. The form of the denominator also indicates that the dependence of the solution on σ_m decreases with decreasing r.

The contrasting behavior of Eqs. (9) and (14) is illustrated in Fig. 2. {In this and several subsequent figures, displays are given of various inversions [solutions of Eqs. (9) and (14)] of signals generated by Eq. (10) in response to specified σ distributions. The value $k = 1$ was used in the computations, except where otherwise indicated. (The choice of k is of course not important so long as the same value is used for generating the signal as for inverting it.)} Figure 2(a) shows the signal response to the platform distribution of σ given

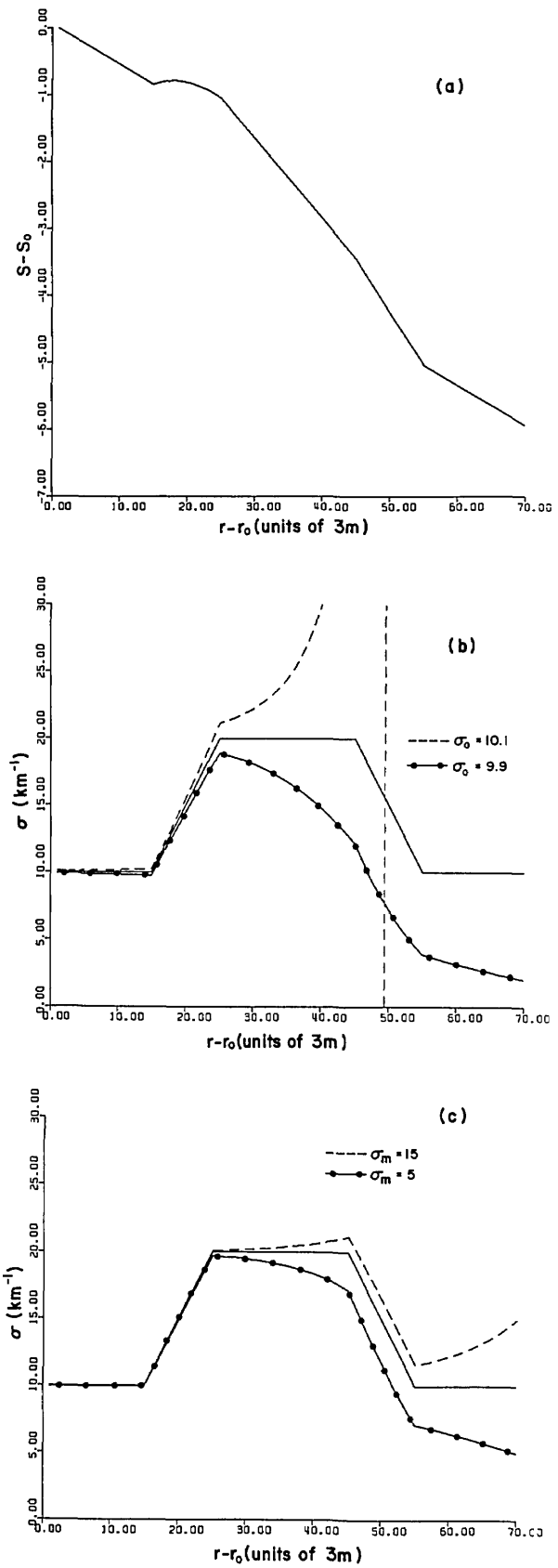

Fig. 2. Effect on inversions of errors in the boundary value estimates of σ.

in Fig. 2(b). Also in Fig. 2(b) are shown the signal inversions from Eq. (9) for boundary values that are in error by ±1%. Figure 2(c) displays the corresponding inversions from Eq. (14) for boundary values that are in error by ±50%. The relatively small effect of a poor boundary value estimate on Eq. (14) is obvious.

Analogous differences in the capacities of the inversions to survive simulated signal noise are shown in Fig. 3. Figure 3(a) shows a noise contaminated signal generated by adding a small background level of noise first to $P(r)$ and then to the resulting $S(r)$. From Eq. (2) it can be seen that as $P(r)$ decreases with range due to attenuation, the weak noise background in P will reveal itself as rapidly increasing noise in S with range. The magnitude of the background noise was chosen to provide an approximate simulation of the limitations in dynamic range of real transient digitizers. (A reviewer, P. B. Russell, provided the inspiration for this particular example.) Thus for a 12-bit digitizer operating under ideal conditions, bit errors become ±100% when $P(r_m)/P_0 = 2^{-12} \approx 2 \times 10^{-4}$. From Eq. (2) we see the corresponding scale of fluctuations induced in S at $r = r_m$ by such bit errors will be $\delta S \approx \delta P/P = 0(1)$, and further that the total decrease in S which can be sustained before the signal is so completely deteriorated is approximately $S_m - S_0 = 2\ln(r_m/r_0) + \ln[P(r_m)/P_0] \approx 2\ln(r_m/r_0) - 8 \approx -6$ for a typical circumstance with $r_m \approx 3r_0$. For the case of a constant attenuation distribution, $\sigma = 10\ \mathrm{km}^{-1}$, shown in Fig. 3, this corresponds to a total range interval of ~300 m.

The inversions of the noisy signal are displayed in Figs. 3(b) and (c). For Fig. 3(b) Eq. (9) was used along with the correct boundary value of attenuation at r_0. The two inversion curves shown illustrate the two possible types of unstable retrievals that result from the use of Eq. (9): if the noise contribution to S at r_0 happens to be positive ($\delta S_0 > 0$), the inversion curve tends unrealistically to decay to zero; on the other hand, if $\delta S_0 < 0$, the inversion curve rises unrealistically with range beyond the point noise is encountered and may even diverge to infinity. [To obtain these outcomes, only the sign of δS_0 was changed; its magnitude, $|\delta S_0| \approx 2 \times 10^{-2}$, is barely detectable on the scale given in Fig. 3(a).] For Fig. 3(c), Eq. (14) was used along with the correct boundary value of attenuation at r_m. The inversion curve illustrates the tendency of Eq. (14) to recover from large signal errors encountered downrange. The result depends negligibly on the sign of δS_0.

The effect of an incorrect value of k is illustrated in Fig. 4, where again the computations are based on the platform-shaped distribution of attenuation shown in Fig. 2, and $k = 1$ was used to generate the signal [shown in Fig. 2(a)]. In Fig. 4(a) it can be seen that as soon as the signal slope varies, so that the value of k enters into the calculations, the inversion based on Eq. (9) fails. The much weaker impact on Eq. (14), illustrated in Fig. 4(b), indicates that great accuracy in the determination of k is not required.

In summary, these examples show that Eq. (14) is relatively insensitive to the kinds of errors that are likely to affect the inversion of real signals. Especially en-

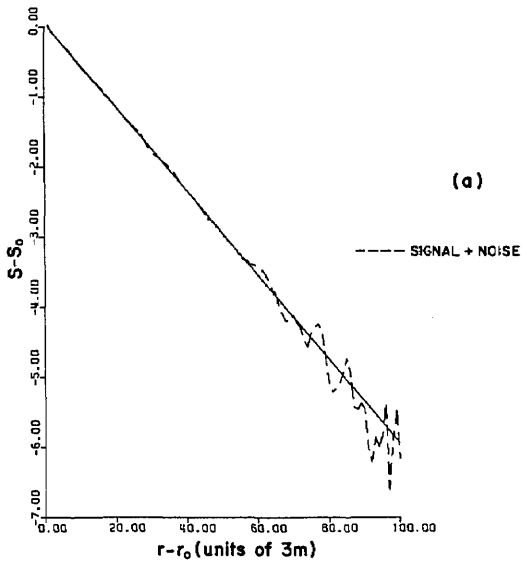

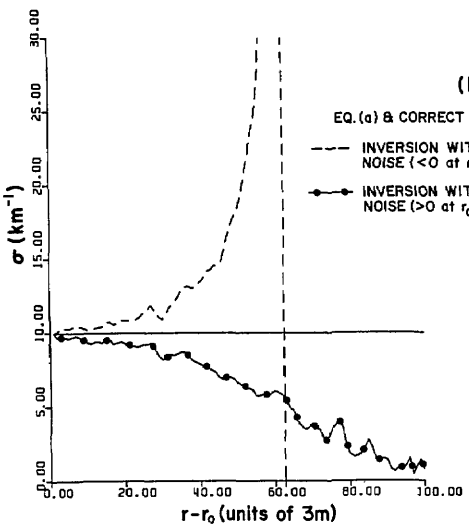

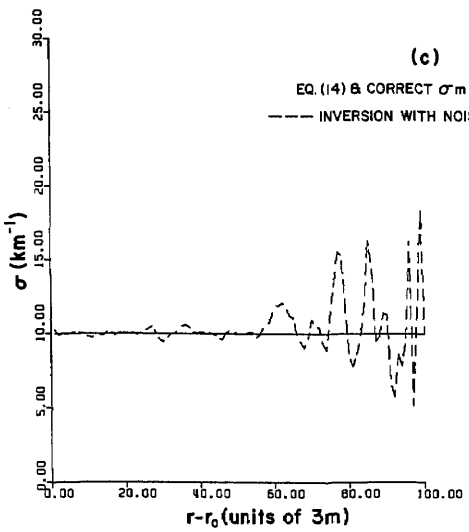

Fig. 3. Effect on inversions of simulated signal noise.

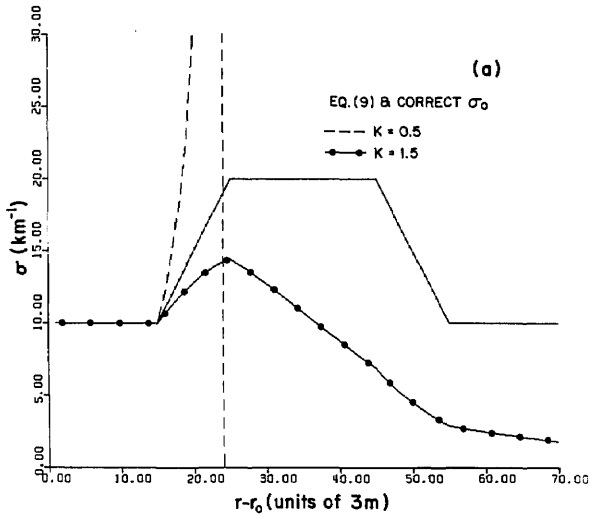

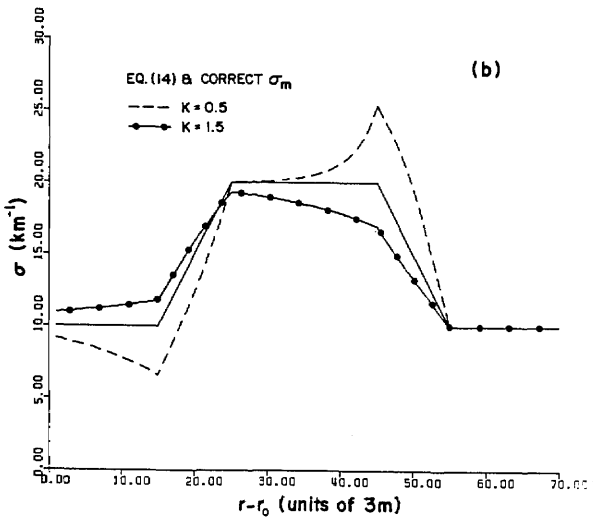

Fig. 4. Effect on inversions of value of k.

couraging is the tendency of Eq. (14) to approach the correct solution curve in spite of a poor estimate of the boundary value σ_m. This raises the hope that difficult accurate lidar calibrations or independent measurements of some optical parameter at a reference point, or through a given layer, may not be necessary, at least for some applications of interest. In the next section, the question of how to make a reasonable self-contained estimate of σ_m from the signal alone is briefly considered.

IV. Estimation of σ_m; Generalization of the Slope Method

It would appear to be a relatively straightforward matter to obtain a good estimate for σ_m in view of the following circumstance: Assuming the validity of the lidar equation, Eq. (1), and the constitutive relation, Eq. (6), and assuming also that σ varies linearly over a specified interval (r_a,r_b), it is possible to express σ solely in terms of the signal over the interval. This follows directly from integration of Eqs. (9) and (14) over (r_a, r_b), with $S_0 \rightarrow S_a = S(r_a)$ and $S_m \rightarrow S_b = S(r_b)$:

$$\int_{r_a}^{r_b} \sigma dr = \frac{-k}{2} \ln\left\{1 - \frac{2\sigma_a}{k} \int_{r_a}^{r_b} \exp[(S - S_a)/k] dr'\right\}, \quad (15)$$

$$\int_{r_a}^{r_b} \sigma dr = \frac{k}{2} \ln\left\{1 + \frac{2\sigma_b}{k} \int_{r_a}^{r_b} \exp[(S - S_b)/k] dr'\right\}, \quad (16)$$

where $\sigma_a = \sigma(r_a)$ and $\sigma_b = \sigma(r_b)$. Because of the assumed linear variation of σ over (r_a,r_b), the average value of σ on the interval is just $\bar{\sigma} = (\sigma_a + \sigma_b)/2$. Therefore, Eqs. (15) and (16) may be combined to predict the values of $\bar{\sigma}$, σ_a, or σ_b. For example, $\bar{\sigma}$ is obtained from the solution of the equation

$$\Omega = \frac{[1 - \exp(-\Omega)]}{2I_{ab}} + \frac{[\exp(\Omega) - 1]}{2I_{ba}}, \quad (17)$$

where

$$\Omega = [2\bar{\sigma}(r_b - r_a)]/k, \quad (18)$$

$$I_{ab} = (r_b - r_a)^{-1} \int_{r_a}^{r_b} \exp[(S - S_a)/k] dr', \quad (19)$$

$$I_{ba} = (r_b - r_a)^{-1} \int_{r_a}^{r_b} \exp[(S - S_b)/k] dr' = I_{ab} \exp[(S_a - S_b)/k]. \quad (20)$$

Since the assumption that σ is linear will become better with decreasing interval size, the application of Eqs. (17)–(20) over a succession of small intervals would appear in principle to constitute an inversion of the lidar signal which does not require any information beyond that contained in the signal itself. In practice, however, the local structure of the signal is not known well enough to ensure the success of such a method. This can be seen by considering the form of the solution to Eqs. (17)–(20) for the case that $\Omega \ll 1$, i.e., for intervals $\Delta r \ll k/2\bar{\sigma}$. By expansion of I_{ab} and I_{ba} to include terms proportional to Δr^2, the solution for $\bar{\sigma}$ is found to be

$$\bar{\sigma} = \frac{-3(S_a' + S_b')}{16} \times \left(1 + \left\{1 - \frac{16}{9(S_a' + S_b')^2}[S_a'^2 + S_b'^2 + k(S_a'' + S_b'')]\right\}^{1/2}\right), \quad (21)$$

where $S_a' = (dS/dr)_{r_a}$, $S_b' = (dS/dr)_{r_b}$, $S_a'' = (d^2S/dr^2)_{r_a}$, and $S_b'' = (d^2S/dr^2)_{r_b}$. This generalization of the slope method result, Eq. (5), is certainly more rigorous in its account of the local geometry of the signal. Unfortunately, however, the new terms representing signal curvature are extremely difficult to estimate, so that point-by-point application of Eqs. (17)–(20) or (21) can generally be expected to provide little real improvement over the slope method.

In view of such difficulties we shall resort here to a very simple slope-type estimate of σ_m, namely,

$$\sigma_m \approx \frac{1}{2} \frac{(S_0 - S_m)}{(r_m - r_0)}. \quad (22)$$

The utility of this expression will increase with increasing optical depth, such that signal variations are caused mainly by changes in attenuation magnitude, rather than by changes in the fractional gradient of attenuation [the first and second terms in Eq. (7)]. For very clean atmospheres it is expected that some additional calibration procedure or other independent means must be invoked to supply an estimate of σ_0 or σ_m.

For turbid atmospheres, if it is known that the attenuation distribution is in a separate regime of nearly constant σ over some subinterval (r_b,r_m) of the total range (r_0,r_m), a better estimate than Eq. (22) may be made by setting $\sigma(r_b) = \sigma_m$ in Eq. (14) and solving for σ_m to obtain

$$\sigma_m \approx \frac{\exp[(S_b - S_m)/k] - 1}{\frac{2}{k} \int_{r_b}^{r_m} \exp[(S - S_m)/k] dr'}. \quad (23)$$

V. Inversion Examples and Discussion

Some examples of inversions generated according to Eqs. (9) and (14), for specified distributions and for various combinations of errors in σ_m or σ_0, S, and k, are shown in Figs. 5–7. In Fig. 5(b) the inversions were obtained from Eq. (14) with σ_m provided by either Eq. (22) or (23). By inspection of the signal in Fig. 5(a) we might expect that the use of the latter equation over $r - r_0 \in (80,100)$ would provide a better estimate of σ_m than Eq. (22). This is confirmed by the results shown in Fig. 5(b). The average value of attenuation over the entire range for the input distribution is $\bar{\sigma}_{in} = 9.7$ km^{-1}, while for the inversions it is $\bar{\sigma}_{out} = 10.7$ km^{-1} using Eq. (22), and $\bar{\sigma}_{out} = 9.8$ km^{-1} using Eq. (23).

A noisy version of the original signal is displayed in Fig. 5(c), the noise contamination having been induced in exactly the same way as described earlier for Fig. 3(a). The resulting inversion via Eqs. (14) and (22) is shown in Fig. 5(d), where it can be seen that the features of the input distribution are still recovered quite well for $r - r_0 \leq 60$. The average value of attenuation for this case is $\bar{\sigma}_{out} = 11.1$ km^{-1}. Corresponding inversions based on Eq. (9), and wherein the correct value of σ_0 is assumed [the results using Eq. (22) with $\sigma_0 = \sigma_m$ would look much worse], are shown in Fig. 5(e); the diverging and decaying inversion forms arise depending on the sign of δS_0, as discussed earlier. As expected, even with exact knowledge of σ_0 and very little noise in the neighborhood of r_0, the inversions provide relatively poor retrievals of the input distribution. For the decaying case, the average attenuation is $\bar{\sigma}_{out} = 6.0$ km^{-1}.

Next we present an example of the additional effects of errors in the assumed relationship between backscatter and attenuation. Consider again the input distribution of attenuation shown in Fig. 5(b). In the previous attempts to retrieve this distribution, Eq. (6) with $k = 1$ was used. Suppose now that the backscatter actually depends more sensitively on the magnitude of σ. A plausible representation of such behavior is to assume a variable k, which departs from unity in proportion to the fractional deviation of σ from its average value, $\bar{\sigma} = 9.7$ km^{-1}; i.e., let $k_2 = 0.5(1 + \sigma/\bar{\sigma})$. For the σ_{in} of Fig. 5(b) the resulting k is shown in Fig. 6(a). On substituting these results into Eq. (10) and adding noise as before, the final signal comes out as displayed in Eq. 6(b). The inversion of this signal assuming Eq. (6) with

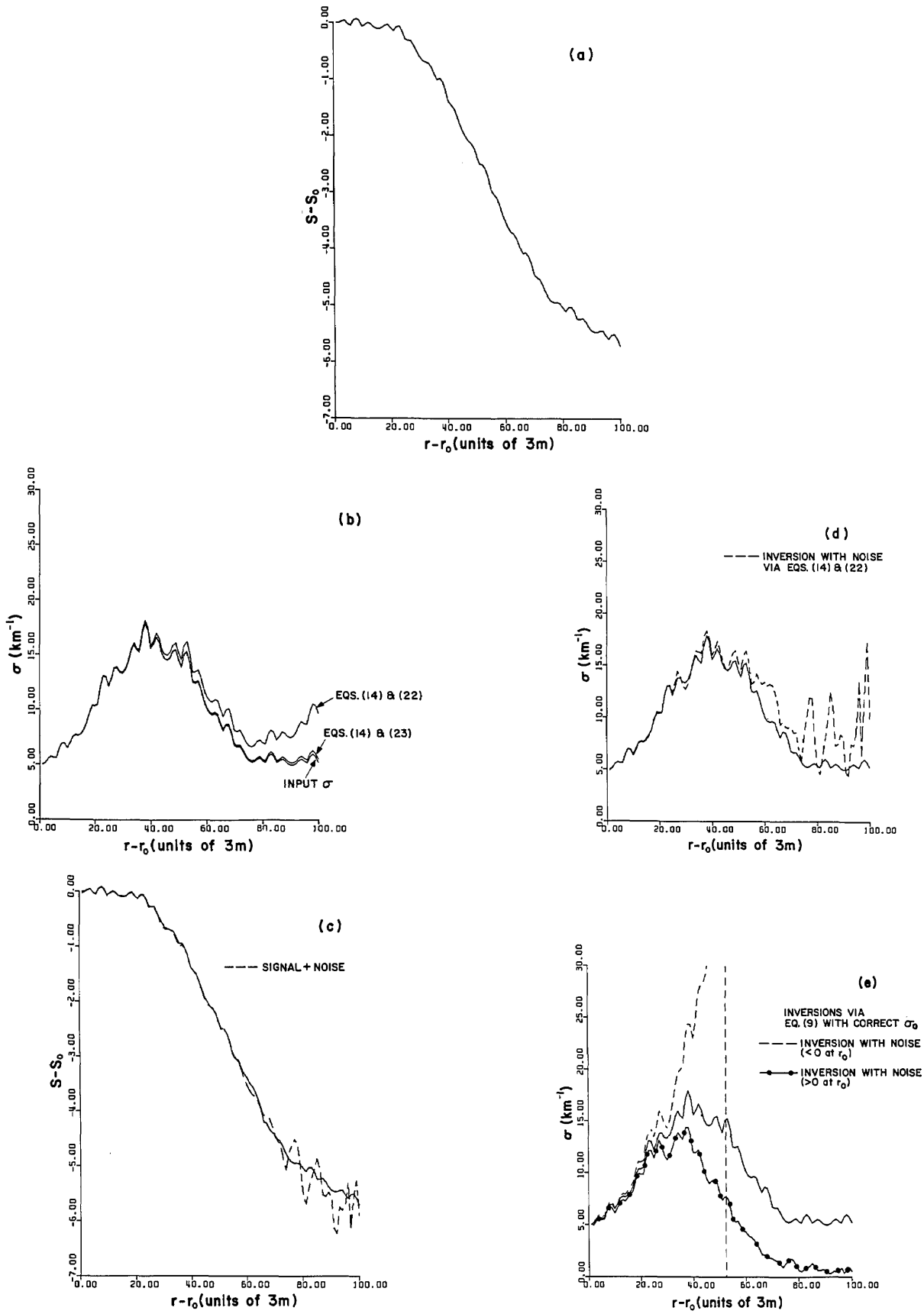

Fig. 5. Inversions for a low visibility strongly inhomogeneous atmosphere, including effects of signal noise.

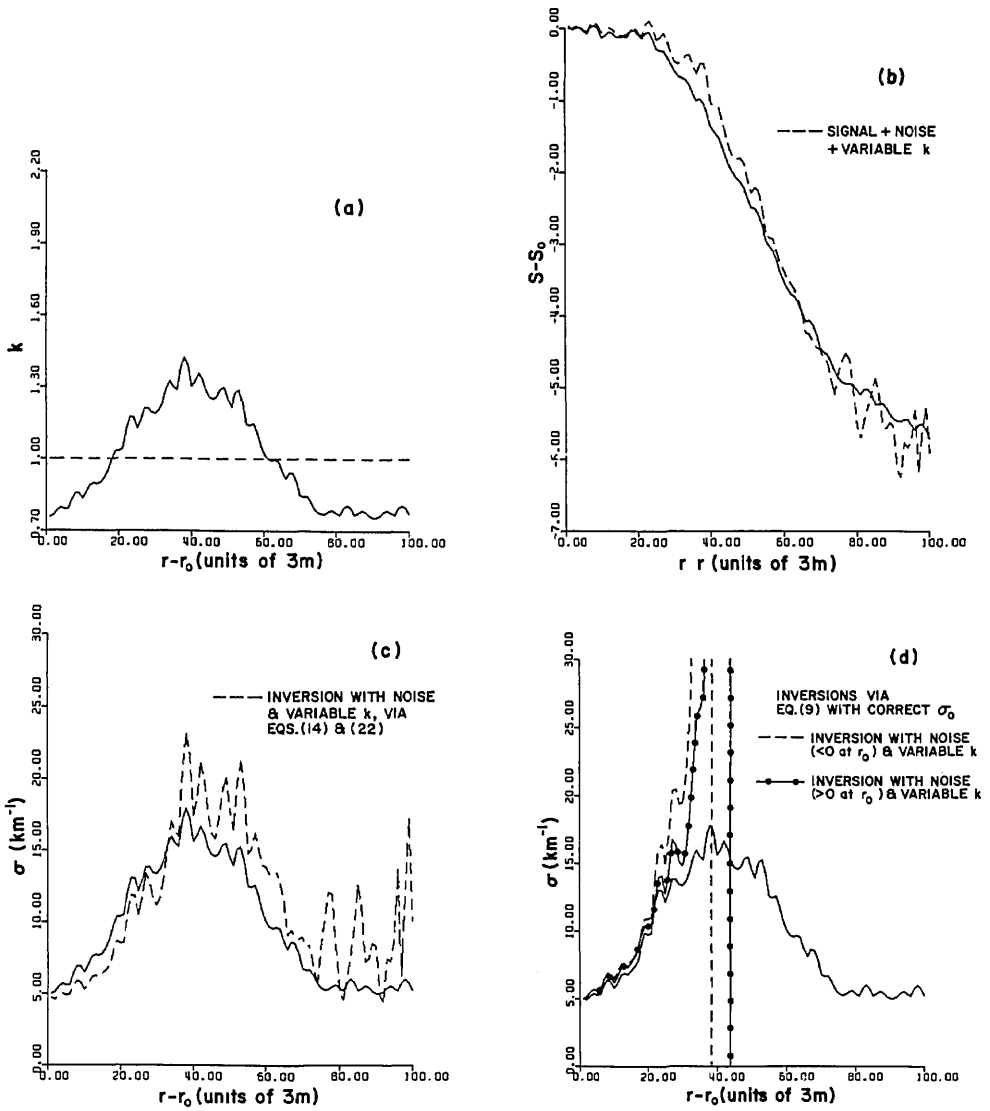

Fig. 6. Same as Fig. 5 but also including effects of variable k.

$k = 1$, Eq. (14), and Eq. (22) is shown in Fig. 6(c). It can be seen that the general features of the input distribution are still recovered fairly well, except in the downrange region of extreme noise. The average value of attenuation for this case is $\bar{\sigma}_{out} = 11.3$ km^{-1}. Corresponding inversions based on Eq. (6) with $k = 1$, Eq. (9), and assuming no errors in the estimate of σ_0, are shown in Fig. 6(d). As in the previous examples, the instability of Eq. (9) is seen to lead to very poor results. A qualitatively new outcome here is that both inversions blow up because of the errors in the assumed relationship between β and σ, regardless of the sign of the signal noise at r_0.

In Fig. 7 an example of a relatively high visibility atmosphere with fairly constant σ is considered. The input distribution of σ is shown best in Fig. 7(d). Effective errors in k are modeled much as in the previous example; owing to the relatively small variation in σ in the present case we set $k = 5(\sigma/\bar{\sigma} - 0.8)$, where now $\bar{\sigma} = 0.57$ km^{-1}. The resulting variation of k with range is displayed in Fig. 7(a). The corresponding signal, including noise contamination as before, is given in Fig. 7(b). In this case the effect of noise as simulated in this paper is relatively unimportant because of the small change in S over the range of interest. The inversion of the signal via Eq. (6) with $k = 1$, Eq. (14), and Eq. (22) is shown in Fig. 7(c). The corresponding inversion assuming Eq. (6) with $k = 1$, Eq. (22) (with $\sigma_0 = \sigma_m$), and Eq. (9) is shown in Fig. 7(d). The average value of attenuation for the inversion based on Eq. (14) is $\bar{\sigma}_{out} = 0.59$ km^{-1}; for Eq. (9) it is $\bar{\sigma}_{out} = 0.63$ km^{-1}.

These results illustrate what is generally true for high visibilities, namely, that there is little to choose between Eq. (9) or (14) in such cases. Obviously, this happens because Eq. (9) is relatively stable for small optical depths. Conversely, small optical depths enhance the tendency of a misfit at the boundary point r_m to carry on through the length of an inversion based on Eq. (14). This effect is not revealed clearly by the example shown in Fig. 7(c), because the estimate of σ_m provided by Eq. (22) happens in this particular case to be very close to the true value. Generally, however, the slope estimate

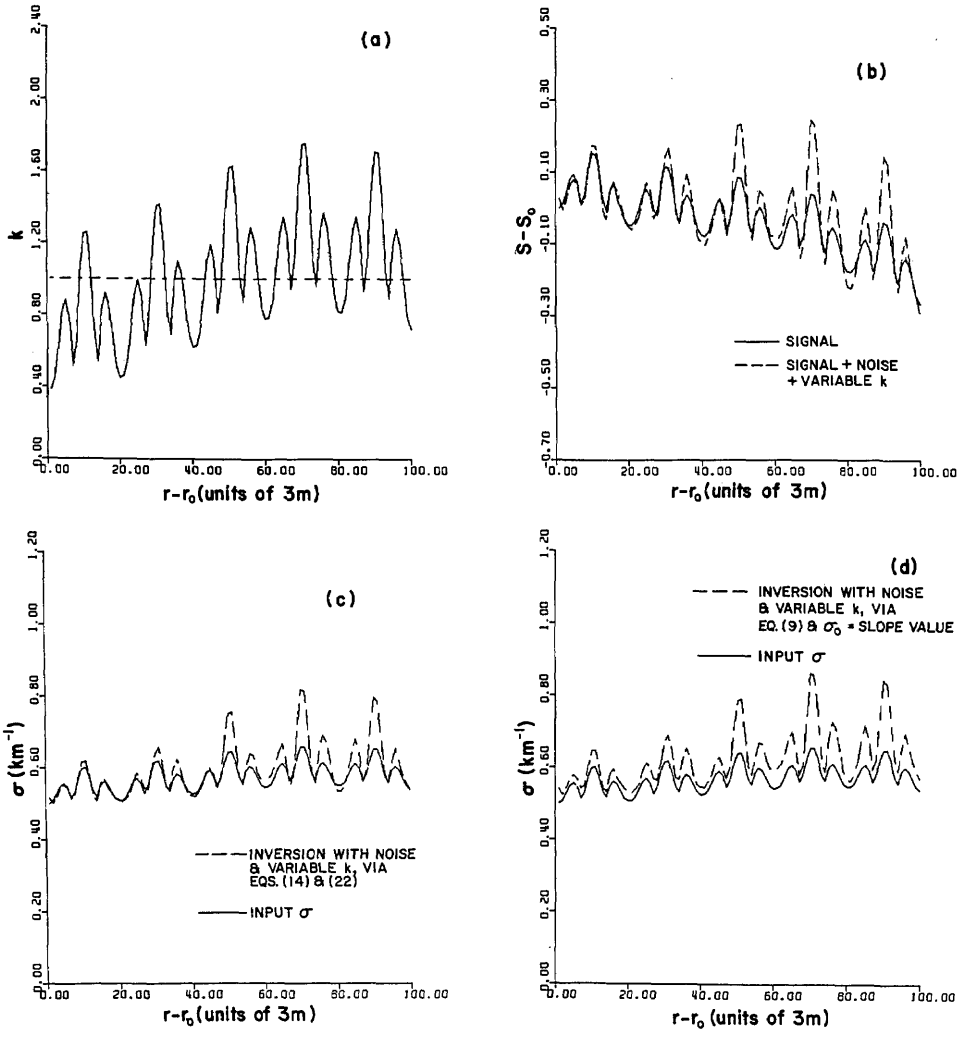

Fig. 7. Inversions for a high visibility atmosphere, including effects of signal noise and variable k.

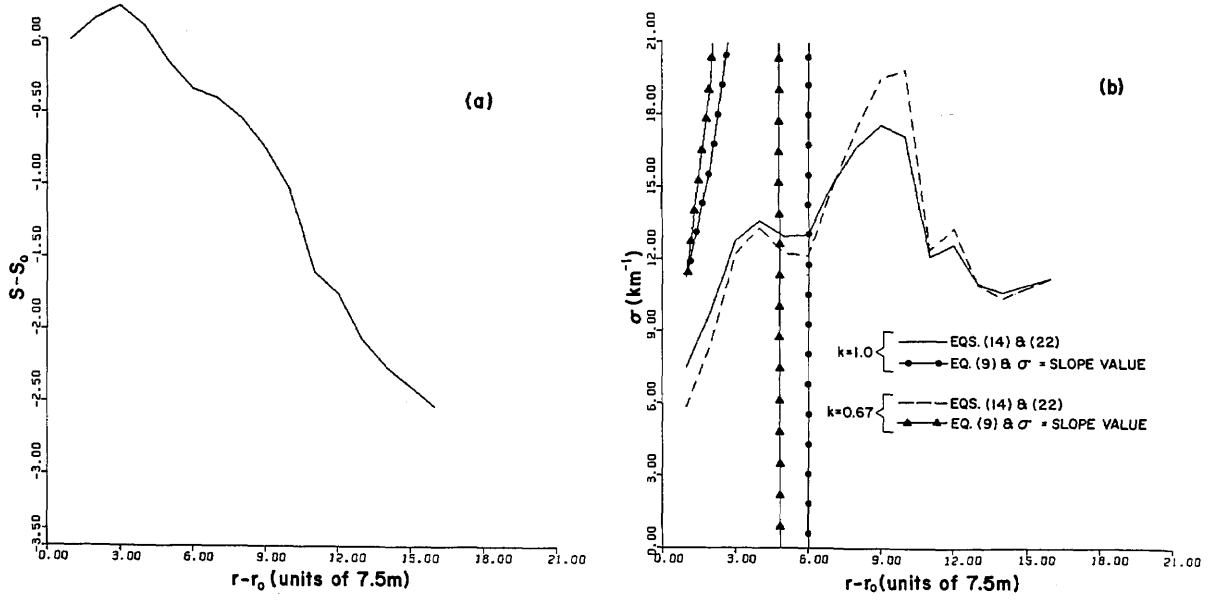

Fig. 8. Inversions of a real lidar signal for $k = 0.67$ and 1.0.

of σ_m will not be very accurate for atmospheres of high visibility, particularly if large fractional changes in σ occur. As indicated earlier, in such cases information beyond that contained in the relative signal, $S - S_0$ vs $r - r_0$, should be supplied.

As a final example, inversions of a real lidar return from fog are shown in Fig. 8. The laser used emitted pulses averaging 10 mJ in 6 nsec at 1.06 μm, and a 20-MHz sampling rate transient recorder was used to produce sample points spaced 7.5 m apart over the lidar return.[27] The initial increase in the lidar signal shown in Fig. 8(a) is due to increasing σ and is not caused by incomplete overlap of the transmitter and receiver fields of view. Inversions based on Eqs. (14) and (22) are shown in Fig. 8(b) for $k = 1.0$ and 0.67; the former value is probably better for fog, but in any case the inversions, as demonstrated earlier, do not depend strongly on the choice of k. For either value of k the average attenuation is $\bar{\sigma} = 13.0\ \text{km}^{-1}$. This result can be compared to the visibility as measured by a transmissometer during the same experiment. The transmissometer visibility $\bar{v}$ (km), based on a contrast threshold of 0.05 so that $\bar{v} = 3.0/\bar{\sigma}$, is 0.20 km.[27] The corresponding value from the lidar inversion is $\bar{v} = 0.23$ km. The extent of agreement is as good as could be expected, given just the uncertainties associated with the experimental data.

Also shown in Fig. 8(b) for comparison are inversions based on Eqs. (9) and (22) (with $\sigma_0 = \sigma_m$). For either value of k the inversions quickly develop singularities. From the values of $\sigma(r_0)$ obtained via Eq. (14) above, it can be seen that the failure of Eq. (9) in this case is due largely to the overestimate of σ_0, which the average slope equation [Eq. (22)] provides.

The support and encouragement of W. J. Lentz and J. S. Randhawa are gratefully acknowledged. Helpful comments by P. B. Russell were also appreciated. This work was performed under contract to the U.S. Army Atmospheric Science Laboratory, White Sands Missile Range, N.M. 88002.

References

1. R. T. H. Collis and P. B. Russell, in *Laser Monitoring of the Atmosphere*, E. D. Hinkley, Ed. (Springer, New York, 1976), p. 117.
2. R. T. H. Collis, Q. J. R. Meteorol. Soc. **92**, 220 (1966).
3. W. Viezee, E. E. Uthe, and R. T. H. Collis, J. Appl. Meteorol. **8**, 274 (1969).
4. H. R. Pruppacher and J. D. Klett, *Microphysics of Clouds and Precipitation* (Reidel, Dordrecht, Holland, 1978), pp. 20–21.
5. T. Okita, J. Meteorol. Soc. Jpn. **40**, 39 (1962).
6. R. T. Brown, Jr., J. Appl. Meteorol. **12**, 698 (1973).
7. W. Viezee, J. Oblanas, and R. T. H. Collis, AFCRL-TR-73-0708, Air Force Cambridge Research Laboratories, Bedford, Mass. (1973), NTIS 776 054.
8. R. H. Kohl, J. Appl. Meteorol. **17**, 1034 (1978).
9. R. H. Kohl, J. Appl. Meteorol. **18**, 712 (1979).
10. R. T. Brown, Jr., J. Appl. Meteorol. **18**, 711 (1979).
11. J. A. Curcio and G. L. Knestrick, J. Opt. Soc. Am. **48**, 686 (1958).
12. R. W. Fenn, Appl. Opt. **5**, 293 (1966).
13. O. D. Barteneva, Bull. Acad. Sci. USSR No. 12, 1, 852 (1960).
14. S. Twomey and H. B. Howell, Appl. Opt. **4**, 501 (1965).
15. R. G. Pinnick, S. G. Jennings, P. Chýlek, and C. V. Hamm, to be submitted to J. Atmos Sci.
16. E. L. Ince, *Ordinary Differential Equations* (Dover, New York, 1956).
17. W. Hitschfeld and J. Bordan, J. Meteorol. **11**, 58 (1954).
18. E. W. Barnett and O. Ben-Dov, J. Appl. Meteorol. **6**, 500 (1967).
19. P. A. Davis, Appl. Opt. **10**, 2099 (1969).
20. F. G. Fernald, B. M. Herman, and J. A. Reagan, J. Appl. Meteorol. **11**, 482 (1972).
21. H. Herrmann, Alta Freq. **9**, 732 (1974).
22. K. N. Liou and R. M. Schotland, J. Atmos. Sci. **28**, 772 (1971).
23. E. W. Eloranta, Ph.D. Thesis, Department of Meteorology, U. Wisconsin (1972).
24. B. M. Golubitskiy, T. M. Zhadko, and M. V. Tantashev, Izv. Atmos. Oceanic Phys. **8**, 1226 (1972).
25. W. G. M. Blättner and C. M. Lampley, Radiation Research Associates Report RRA-47706, Fort Worth, Tex. (1977).
26. I. V. Samokhvalov, Opt. Lett. **4**, 12 (1979).
27. R. S. Bonner and W. J. Lentz, Atmospheric Sciences Laboratory Report ASL-TR-0042, White Sands Missile Range, N.Mex. (1979).

Dudley Williams of Kansas State U. (left) and Fred Nicodemus of National Bureau of Standards, photographed by F. S. Harris, Jr. (U. Utah) during the 1980 OSA Annual Meeting.